Front depinning by deterministic and stochastic fluctuations: A comparison

A. J. Alvarez-Socorro,[1] Marcel G. Clerc,[1] M. A. Ferré,[1] and Edgar Knobloch[2]

[1]*Departamento de Física and Millennium Institute for Research in Optics, Facultad de Ciencias Físicas y Matemáticas,*
Universidad de Chile, Casilla 487-3, Santiago, Chile
[2]*Department of Physics, University of California at Berkeley, Berkeley, California 94720, USA*

Driven dissipative many-body systems are described by differential equations for macroscopic variables which include fluctuations that account for ignored microscopic variables. Here, we investigate the effect of deterministic fluctuations, drawn from a system in a state of phase turbulence, on front dynamics. We show that despite these fluctuations a front may remain pinned, in contrast to fronts in systems with Gaussian white noise fluctuations, and explore the pinning-depinning transition. In the deterministic case, this transition is found to be robust but its location in parameter space is complex, generating a fractal-like structure. We describe this transition by deriving an equation for the front position, which takes the form of an overdamped system with a ratchet potential and chaotic forcing; this equation can, in turn, be transformed into a linear parametrically driven oscillator with a chaotically oscillating frequency. The resulting description provides an unambiguous characterization of the pinning-depinning transition in parameter space. A similar calculation for noise-driven front propagation shows that the pinning-depinning transition is washed out.

I. INTRODUCTION

Nonequilibrium systems, i.e., driven dissipative systems, frequently exhibit rich and complex interface dynamics as one state displaces another or defects nucleate, drift, and annihilate [1–4]. This defect evolution is usually dominated by interface, wall, or front dynamics depending on the physical context under study. These nonlinear waves do not obey the superposition principle, and each interface has a well-defined profile that depends on the parameter values of the system. The concept of front propagation originally emerged in the context of population dynamics [5], gene propagation [6] as well as flame propagation [7], and has since attracted growing interest in chemistry, biology, physics, and mathematics [1–3,8].

In physics, fronts play a central role in a large variety of situations, ranging from reaction-diffusion models and solidification processes to pattern-forming systems arising in fluid dynamics (see, e.g., [1,3,9] and references therein). From the point of view of dynamical systems theory a one-dimensional front of constant form corresponds to a heteroclinic orbit connecting two spatially extended homogeneous states [10]. The propagation speed of the front depends on the type and stability of the states connected by the front. One of the most studied types of front is that connecting a stable spatially homogeneous state with an unstable one, the so-called FKPP or pulled front [2,11]. The speed of such a front is not, in general, unique and depends on the initial condition [11]. Another well-known type of front, a bistable or pushed front, connects two stable homogeneous states [4]. Such fronts are found inside a bistability region between two homogeneous states and are characterized by a single speed that is determined by the free energy difference between the two states whenever the system is variational. In this case the state with the lower energy displaces that with higher energy [4] and the

front speed only vanishes at the Maxwell point, at which both states have the same energy [1].

The previous scenario changes when the front connects a homogeneous state to a spatially periodic or patterned state. As first pointed out by Pomeau [4], the presence of spatial heterogeneity is expected to generate an energy barrier or pinning potential that has to be overcome before the front can propagate, i.e., front propagation only occurs when the energy difference between the two states exceeds a nonzero minimum value. In the vicinity of the Maxwell point the energy difference is too small for propagation and the front remains motionless or pinned. When the energy difference is large enough and the front depins, it moves in a stick-slip manner, with a mean speed that increases as the square root of the distance from the parameter value for depinning. The existence of a pinning range has been discussed in a number of physical contexts, and in particular in the context of the generalized Swift-Hohenberg model [12] and the crystallization kinetics of cellular patterns (see the textbook [1] and references therein). Experimentally, an observation of the pinning-depinning transition in a spatially periodic optical medium was reported in [13]. However, the inclusion of inherent incoherent fluctuations (i.e., noise) drastically changes the pinning-depinning transition [14,15]. Noise-induced escape over the confining potential barrier [16] allows the system to escape permanent pinning and ultimately always results in front propagation. Likewise, one can consider fronts that connect a state with coherent intrinsic spatiotemporal fluctuations (chaos, spatiotemporal chaos, turbulence, etc.) with a nonfluctuating homogeneous state. This type of front is fundamental to the understanding of flame propagation in combustion [17–19], emergence of turbulence in pipe flow [20], turbulence propagation [21], and the propagation of spatiotemporal chaos in an optical fiber cavity [22,23]. However,

in these systems no pinning-depinning transition is observed. In contrast, phase-coupled oscillators with a nonlocal coupling exhibit states with partial synchrony called chimera states. These states can be considered to be bound states of a pair of synchronization fronts bounding a coherent state, embedded in a background incoherent state [24–28]. Despite the fluctuations in the background these fronts do not depin and the length of the interval of coherence fluctuates about a well-defined mean determined by the parameters of the problem.

Incoherent fluctuations, such as those arising from thermal effects, are usually described by a random variable having equal intensity at different frequencies (white noise), i.e., a constant power spectrum density [29]. Thus, fluctuations of any size are allowed, with the restriction that large fluctuations are unlikely. In contrast, deterministic (chaotic) fluctuations have a power spectrum dominated in general by certain incommensurate frequencies [30]. Moreover, since the strange attractor responsible for the chaos is typically bounded, the associated deterministic fluctuations have a maximum size. This difference between the accessible deterministic and stochastic fluctuations has a major impact on the dynamics of fronts.

The basic question is whether coherent spatiotemporal fluctuations always trigger a depinning transition in systems exhibiting pinned fronts between two distinct states, in other words whether deterministic fluctuations behave like additive noise [16]. We show here that in the presence of coherent spatiotemporal fluctuations fronts between a spatiotemporally chaotic pattern and a homogeneous state may indeed remain pinned, albeit in a narrower parameter range. We also show, using a bistable model that exhibits a pinning-depinning transition driven by phase turbulence, that this transition is robust but that the pinning-depinning boundary becomes complex, generating a fractal-like structure in parameter space. We describe the pinning-depinning transition using an effective equation for the front position which takes the form of an equation for an overdamped system with a ratchet potential and chaotic forcing determined by the instantaneous location of the front. These fluctuations are bounded and may be insufficient to trigger a depinning transition. Using a series of transformations we convert this problem into a linear parametrically driven oscillator with a chaotically oscillating frequency. The resulting description allows us to characterize the pinning-depinning transition unambiguously, by identifying the unbounded (bounded) solutions of the oscillator problem with pinned (depinned) solutions of the front problem, and hence allows us to compute the boundary between the two, i.e., the location in parameter space of the pinning-depinning transition. A similar calculation for a noise-driven system leads to the same ratchet potential but driven by additive white noise. In this case the front always eventually depins.

II. MODEL

To investigate the propagation of an interface between homogeneous and complex spatiotemporal states, we consider the following model:

$$\partial_t u = u(\alpha - u)(u - 1) + \partial_{xx} u + \beta u \cos(kx) + \gamma u \partial_x \psi, \quad (1)$$

where $u(x, t)$ is a scalar field. The first term on the right-hand side describes a bistable system and corresponds to the Nagumo nonlinearity in the context of population dynamics [8]. The second term accounts for diffusion. The third term represents spatial forcing with amplitude β and wavelength $\lambda = 2\pi/k$ which gives rise to a pattern state. Finally, the last term represents multiplicative spatiotemporally chaotic forcing, with the auxiliary scalar field ψ taken to satisfy the Kuramoto-Sivashinsky equation

$$\partial_t \psi = -\mu \partial_{xx} \psi - (\partial_x \psi)^2 - \partial_{xxxx} \psi. \quad (2)$$

Equation (2) describes the propagation of nonlinear waves of chemical concentration in the Belousov-Zhabotinskii reaction [32–34] and the propagation of flame fronts [35,36], and is perhaps the simplest model that exhibits spatiotemporal chaos [37]. In this context, $\psi(x, t)$ determines the position of an interface between two distinct states. In this paper we use this equation to provide spatiotemporal forcing of Eq. (1) via the zero-mean coupling term $\partial_x \psi$. Note that the field $u(x, t)$ does not feed back on $\psi(x, t)$. Thus, the spatiotemporal forcing is *prescribed*. A model similar to Eqs. (1) and (2) was originally introduced to understand the existence of localized but spatiotemporally chaotic solutions [31].

The unforced Eq. (1), $\beta = \gamma = 0$, corresponds to the well-known Nagumo model [8,38]. This model has two stable homogeneous states $u = 1$ and $u = 0$ that may be connected by a front. Such fronts are typically nonstationary and so propagate with a speed that depends on the value of the parameter α ($0 < \alpha < 1$). Thus α measures the relative stability of the two competing states: for $\alpha < 1/2$ (respectively, $\alpha > 1/2$), the state $u = 1$ (respectively, $u = 0$) takes over the system. There is only one value of α, $\alpha \equiv \alpha_M = 1/2$, at which the interface is motionless. This particular value of α is called the Maxwell point [1]. When the spatial forcing is taken into account ($\beta \neq 0$, $\gamma = 0$), the above scenario changes. Although the state $u = 0$ persists unchanged, the state $u = 1$ is replaced by a periodic state with imprinted wavelength $2\pi/k$, cf. [13,39,40]. Hence, in this parameter regime, the system possesses fronts between a periodic solution and a homogeneous state, a situation that is conducive to front pinning [4]: the presence of spatial heterogeneity generates an energy barrier that must be overcome before the front can move. Consequently, the front speed vanishes over a relatively large interval of parameters, the so-called *pinning range*. Figure 1(a) shows a typical pinning range as a green shaded area. Square symbols (■) represent the numerically determined average front speed. The plot shows that the pinning-depinning transition corresponds to a supercritical bifurcation that takes place at $\alpha_c = \alpha_\pm$. These critical points correspond to SNIPER (Saddle-Node In a PERiodic orbit) bifurcations as found in related depinning problems [41]. Indeed, the average front speed, $\langle V \rangle$, grows as the square root of the distance from the critical point, $\langle V \rangle \sim \sqrt{|\alpha - \alpha_\pm|}$. Far from this critical point, the average front speed grows linearly [42]. The resulting bifurcation diagram was verified experimentally in a spatially forced liquid crystal light valve experiment [13,39].

When $\gamma \neq 0$ the pattern state around $u = 1$ becomes spatiotemporally chaotic and as a result the pinning range shrinks [Fig. 1(a)]. The pinning interval that remains decreases as the forcing wave number k increases [Fig. 1(b)], and vanishes in a
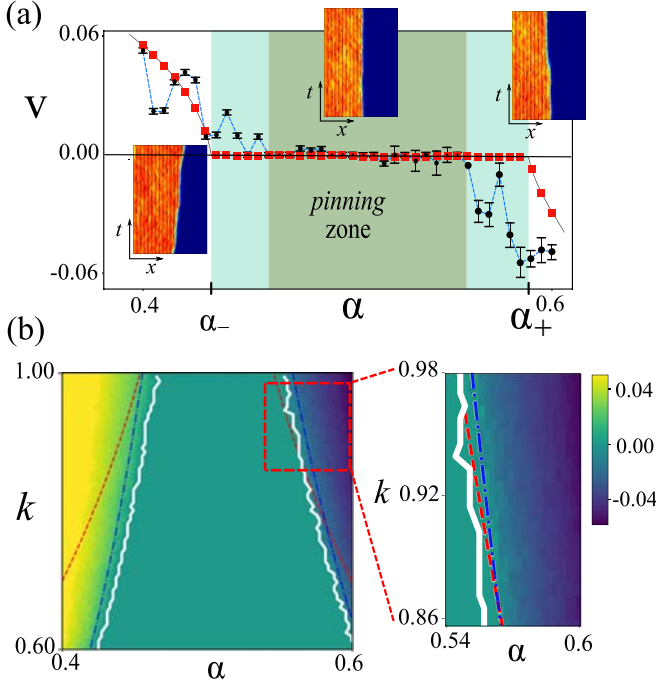
FIG. 1. Pinning-depinning transition of spatiotemporally chaotic patterns embedded in a stable homogeneous state. (a) Average front speed $\langle V \rangle$ as a function of α. The filled squares (■) and circles (●) represent the average speed of the front obtained from numerical simulations of Eqs. (1) and (2) with $\beta = 0.085$, $k = 0.7$, and, respectively, $\gamma = 0$ and $\gamma = 0.055$. The vertical bars show the standard deviation of the front speed. The pinning region for $\beta \neq 0$ and $\gamma = 0$ is shown using light shading. This region shrinks as a result of spatiotemporally chaotic forcing, $\gamma \neq 0$ (dark shaded region). The insets show the spatiotemporal dynamics of the fronts in different parameter regimes. (b) Pinning region in the (α, k) parameter space. The white curve represents the boundary of the pinning region of the spatiotemporally forced model (1) and (2) with $\beta = 0.085$, $\gamma = 0.055$ computed numerically. For comparison we also show the location of the theoretically predicted pinning-depinning transition $\alpha_{\pm} = \alpha_M \pm \sqrt{\beta k A(k)/2}$ with $\alpha_M = 1/2$ and $A(k)$ determined from formula (10) (red dashed line) and from numerical integration of the interface equation (8) (blue dashed-dotted line). Both procedures are valid for $\gamma \ll 1$ only. The quality of the theoretical predictions can be ascertained from the enlargement shown in the lower right panel.

cusp at $(\alpha, k) = (1/2, \infty)$ as $k \to \infty$ (not shown). Figure 2(a) shows a typical spatiotemporal evolution of the chaotic pattern state. This state may be characterized by means of Lyapunov exponents, which provide information about the solution sensitivity to exponentially close initial conditions [43]. From a dynamical systems point of view, if the largest Lyapunov exponent is positive, the system is chaotic, but not necessarily spatiotemporally chaotic. To distinguish between these two types of complex dynamical behavior, it is necessary to compute the Lyapunov spectrum, i.e., the set of Lyapunov exponents [43,44]. Spatiotemporal chaos has a Lyapunov spectrum with a continuous set of positive values. In this case, the number of positive exponents in the Lyapunov spectrum depends on the length L of the domain. In contrast, chaos in a low-dimensional system possesses a Lyapunov spectrum with a discrete set of positive exponents whose number is
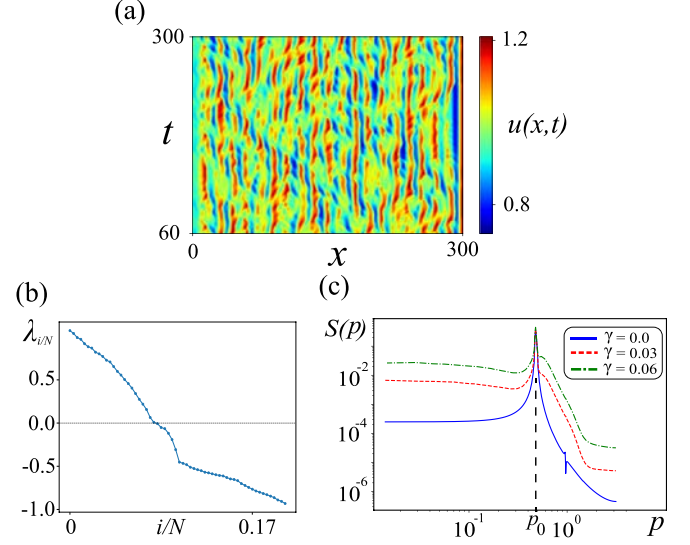

FIG. 2. Spatiotemporally chaotic pattern state of the Kuramoto-Sivashinsky-Nagumo model, Eqs. (1) and (2), when $\alpha = 0.38$, $\beta = 0.085$, $\gamma = 0.03$, and $k = 0.6$. (a) Space-time diagram. (b) The corresponding Lyapunov spectrum. (c) Power spectra $S(p)$ of the pattern state $u(x, t)$ for three different values of the forcing amplitude γ averaged over $T = 10^6$ snapshots. The forcing wave number k is denoted by p_0.

independent of L. Figure 2(b) shows the Lyapunov spectrum of the spatiotemporally chaotic pattern state in Fig. 2(a), computed from Eqs. (1) and (2) using the strategy proposed in [45,46]. Here, N counts the number of points into which the system has been discretized and i is an integer that indexes the Lyapunov exponents. The figure shows that this state is indeed spatiotemporally chaotic. All the numerical simulations were conducted using finite differences for spatial discretization and a fourth-order Runge-Kutta method for the time evolution. Neumann boundary conditions were imposed on both the Nagumo-Kuramoto and the Kuramoto-Sivashinsky equations. The domain length was fixed at $L = 300$ with a space discretization interval $dx = 0.6$ and time step $dt = 0.01$ for the time evolution.

With the aim of understanding the mode dynamics of the state shown in Fig. 2(a), we introduce the time-averaged power spectrum [37]

$$S(p) = \frac{1}{T} \int_0^T \left| \int_0^L u(x, t) e^{ipx} dx \right|^2 dt, \qquad (3)$$

where L is the system size and T is a large time interval. The resulting spectra, computed from Eqs. (1) and (2) for several different values of the forcing amplitude γ, are shown in Fig. 2(c) and confirm the broad-band nature of the mode-mode interactions involved in the spatiotemporally chaotic state despite the dominance of the forcing wave number $p_0 = k$ and its harmonics.

From Fig. 1 and the related results in Fig. 2 we infer that the model (1) and (2) exhibits coexistence between a spatiotemporally chaotic pattern $u(x, t)$ and the homogeneous state $u = 0$. Under these conditions one expects to find front solutions between these states. The insets in Fig. 1(a)
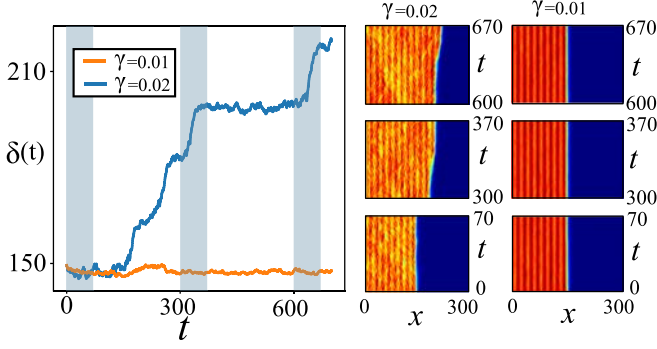
FIG. 3. Temporal evolution of the front position $x = \delta(t)$ in the model (1) and (2) in the pinning and depinning regimes when $\alpha = 0.45$, $\beta = 0.085$, $k = 0.9$, and $\gamma = 0.01$ (pinned front, right panel) and $\gamma = 0.02$ (unpinned front, middle panel).

FIG. 4. Largest Lyapunov exponent λ_{LLE} of the front position as a function of α for $k = 0.7$, $\gamma = 0.055$, and $\beta = 0.085$. The shaded region shows the pinning region.

depict typical front solutions of this type and their temporal evolution for different values of the parameter α. The filled circles (●) in Fig. 1(a) represent the average front speed computed numerically and these show that for $k = 0.7$ and $\gamma = 0.055$ the pinning-depinning transition not only persists but also acquires complex dependence on the forcing wave number k.

To characterize the dynamics of the front in greater detail, we monitored its position $x = \delta(t)$ defined by the condition

$$\delta(t) \equiv \frac{\int_{-L/2}^{L/2} x \, \partial_x u(x,t) \, dx}{\int_{-L/2}^{L/2} \partial_x u(x,t) \, dx}, \tag{4}$$

where L is the system size. Thus $\delta(t)$ corresponds to a value of the field $u(x,t)$ between the two equilibria. In particular, in the unperturbed problem $u(x = \delta) = 1/2$, a value exactly halfway between the two equilibria. Figure 3 illustrates the temporal evolution of the front position in the pinning and depinning regimes, respectively. As a result of chaotic forcing the pinning-depinning boundary becomes complex, generating a fractal-like structure [see Fig. 1(b), white curve]. Complex fluctuations around a given location characterize the front position inside of the pinning region (see Fig. 3, dark orange curve). Outside of the pinning region, the front position exhibits stick-slip dynamics with complicated oscillations around a fixed position alternating with jumps to a new position. This process repeats, with jumps of order of the wavelength $2\pi/k$ and always in the same direction (see Fig. 3, dark blue curve). The complexity of the front motion can be quantified in terms of the largest Lyapunov exponent which characterizes the behavior of the sudden jumps in the front position $\delta(t)$ as parameters are varied in the spatiotemporally chaotic regime [43]. Figure 4 shows the largest Lyapunov exponent, λ_{LLE}, of this motion, computed from 200 slightly different initial conditions, as a function of the parameter α. The exponent λ_{LLE} tends to increase with increasing α but cannot be used to infer the location of the pinning region. In other words, the chaotic behavior inside and outside of the pinning region exhibits similar characteristics, and λ_{LLE} is not a good indicator of the pinning-depinning transition.
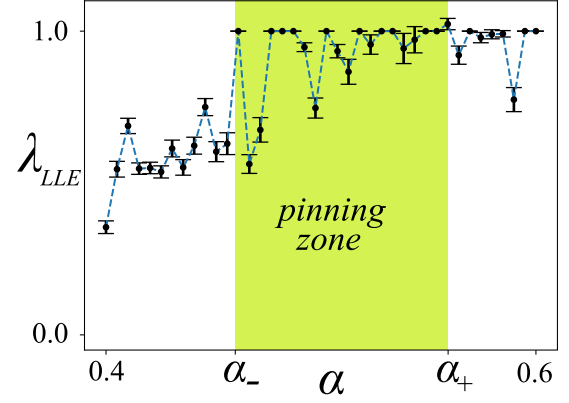
III. ANALYTICAL CHARACTERIZATION OF INTERFACE DYNAMICS

In this section, we explain the pinning-depinning transition in terms of the front position $\delta(t)$. An equation describing the dynamics of δ is deduced using perturbation methods. Similar approaches have been used to explain the existence of both stationary [42] and time-dependent [31] localized structures.

The unforced model, Eqs. (1) and (2) with $\beta = \gamma = 0$, has an exact stationary front solution at the Maxwell point $\alpha_M = 1/2$ connecting the two homogeneous states $u = 0$ and $u = 1$:

$$u_F(x, \delta) = \frac{1}{2} + \frac{1}{2} \tanh\left(\frac{\sqrt{2}}{4}(x - \delta)\right). \tag{5}$$

To understand the effect of spatial ($\beta \neq 0$) and spatiotemporally chaotic ($\gamma \neq 0$) forcing, we suppose that both β and γ are small and that the system is close to the Maxwell point, i.e., $\gamma \sim \beta \ll 1$ and $\tilde{\alpha} \equiv \alpha_M - \alpha$, with $\tilde{\alpha} \sim \gamma \sim \beta$. Let us consider the following ansatz:

$$u(x, t) = u_F(x - \delta(t)) + W(x, t), \tag{6}$$

where the front position $\delta(t)$ is promoted to a temporal function representing the dynamics of the interface. The remainder term $W(x, t)$ is assumed to be small, of the order of β, γ, and $\tilde{\alpha}$. Introducing the above ansatz in Eq. (1) together with the definition of the comoving coordinate $z \equiv x - \delta(t)$, and linearizing in W, we obtain

$$-\mathscr{L}W = \partial_z u_F \dot{\delta} - \tilde{\alpha} u_F(u_F - 1) + \beta u_F \cos(kz + k\delta) + \gamma u_F \partial_z \psi(z + \delta, t), \tag{7}$$

where the linear operator $\mathscr{L} \equiv 3u_F - 3u_F^2 - 1/2 + \partial_{zz}$. To solve the above linear equation, we introduce the inner product $\langle f|g\rangle = \int_{-\infty}^{\infty} f^*(z)g(z)dz$. Using this inner product, it is easy to show that $\mathscr{L}$ is self-adjoint, $\mathscr{L} = \mathscr{L}^\dagger$. Note that $\partial_z u_F$ is an element of the kernel of $\mathscr{L}^\dagger$. Applying the solvability condition, equivalently the Fredholm alternative [47], one obtains, after straightforward calculations,

$$\dot{\delta} = -\frac{\partial U}{\partial \delta} - 6\sqrt{2}\gamma B(t). \tag{8}$$

The first term is the gradient of an effective time-independent potential given by

$$U(\delta) \equiv \sqrt{2}\tilde{\alpha}\delta + \beta A \sin(k\delta + \phi), \qquad (9)$$

where

$$A \equiv 6\pi\sqrt{1 + 2k^2}\,\text{csch}(\sqrt{2}\pi k), \qquad (10)$$

$$\phi \equiv \arctan(\sqrt{2}k). \qquad (11)$$

The potential $U(\delta)$ in Eq. (9) is called a washboard potential or equivalently a *generalized Peierls-Nabarro potential* because of its use in describing the dynamics of dislocations in crystals [48–50]. However, it also describes the motion of charged particles in a periodic crystal in the presence of an electric field, and arises in other spatially forced physical systems as well. In particular, the potential has been used to explain the existence of localized spatiotemporally chaotic solutions in both continuous [31] and discrete media [27,51].

The second term on the right-hand side of Eq. (8) corresponds to additive time-dependent forcing with amplitude

$$B(t) \equiv \int_{-\infty}^{\infty} u_F(z)\partial_z u_F(z)\partial_z \psi(z + \delta, t)\,dz. \qquad (12)$$

Although this chaotic forcing appears to depend on the front position δ this fact does not change the statistical properties of B(t) which remain on average homogeneous.

Equation (8) describes an overdamped system with a ratchet potential and chaotic forcing. When the potential barrier between equilibria is sufficiently large the front position fluctuates around an equilibrium position and we call the front pinned. On increasing the forcing amplitude γ above a critical value, the front position begins to explore nearby equilibria in order to minimize energy, leading to a pinning-depinning transition, i.e., to the onset of front propagation. Thus front propagation corresponds to a *chaotic ratchet motor*.

In the absence of spatiotemporally chaotic forcing, $\gamma = 0$, an analytical expression for the pinning-depinning transition can be deduced from the stationary solution of Eq. (8). The width of the pinning region is determined by the condition $A^2(k) = 2\tilde{\alpha}^2(k)k^2/\beta^2$. Figure 1(b) shows the smooth dependence of the resulting pinning-depinning transition $\alpha_{\pm}(k)$ on the wave number k (dashed red line).

When spatiotemporally chaotic forcing is included, $\gamma \neq 0$, the pinning-depinning boundary $\alpha_{\pm}(k)$ is fundamentally altered, and now takes on a fractal structure. In Fig. 1(b) this boundary is indicated by the white curve. To understand the complex dynamics exhibited by the fronts near this boundary and the complex structure of the boundary in parameter space, one must first characterize the spatiotemporally chaotic forcing given by Eq. (12). Figure 5 shows the temporal evolution of the function B(t) obtained from the Kuramoto-Sivashinsky model (2) with $\mu = 3.0$. The statistical characterization of the spatiotemporally chaotic forcing and its probability density function can be determined from Eq. (2), and is shown in Fig. 5(b). Note that the histogram of the values acquired by the function B(t) is similar to a Gaussian distribution [the fit in Fig. 5(b) has standard deviation 0.2355] although the distribution has compact support (see the zoom of the histogram tail). This is a consequence of the fact that the function $\partial_z u_F(z)$ in the integrand in Eq. (12) cuts off
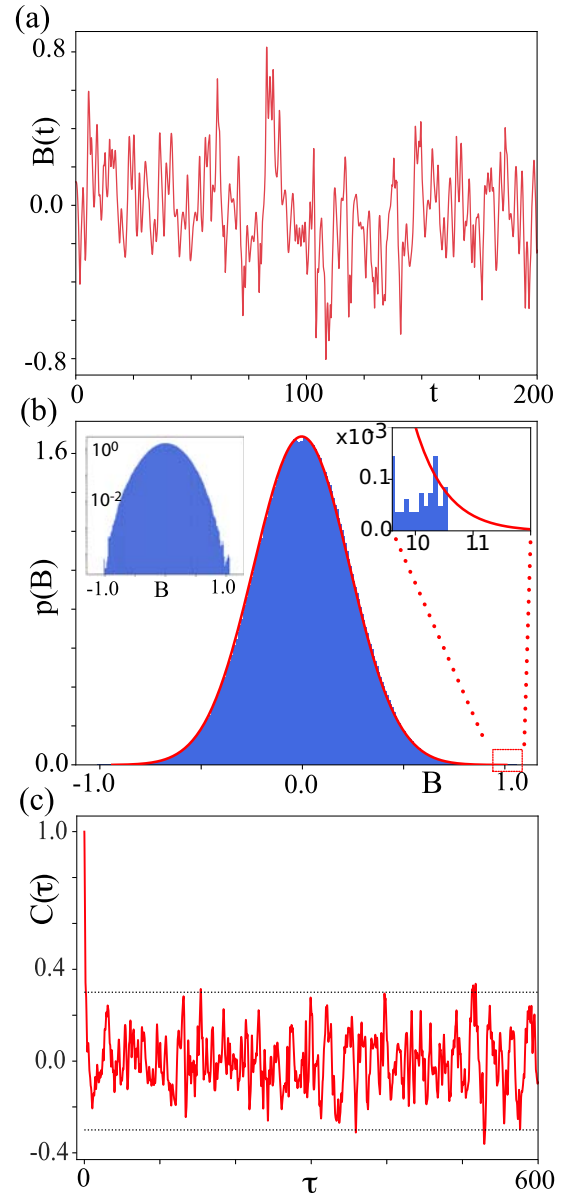

FIG. 5. Statistical characterization of the spatiotemporally chaotic forcing term B(t) in Eq. (12). (a) Typical temporal evolution of B(t) obtained from the Kuramoto-Sivashinsky forcing (2) with $\mu = 3.0$ and domain length $L = 300$, computed with a discretization interval $dx = 0.6$ and time step $dt = 0.01$. (b) Probability density function of B(t) in terms of a histogram (blue columns). The red curve represents a Gaussian fit. The left inset displays the probability density function of B(t) in a semi-log plot, while the right inset shows the tail of the histogram, suitably magnified, showing the truncation of the distribution. (c) Correlation function $C(\tau) \equiv \langle B(t)B(t + \tau)\rangle$, where the symbol $\langle\cdot\rangle$ denotes an average over the time t.

the contributions from the spatiotemporally chaotic process $\partial_z \psi(z, t)$ at large $|z|$, implying that B(t) does not behave as an infinite sum of independent identically distributed random variables. Consequently, B(t) is not a Gaussian white noise, a fact confirmed by the correlation function $C(\tau)$ shown in Fig. 5(c). This correlation function does not decay to zero as $\tau \to \infty$, in contrast to a genuine stochastic process.

In the following we explore the consequences of the above finding.

IV. PINNING-DEPINNING TRANSITION AS A PARAMETRIC RESONANCE

The pinning-depinning transition of a front can be understood as a parametric resonance [52]. To see this we transform Eq. (8) into a linear parametric oscillator equation using a series of nonlinear changes of the dependent variable $\delta(t)$. The effective frequency of the resulting oscillator problem fluctuates chaotically as a result of the spatiotemporally chaotic forcing. In order to identify the threshold for the transition in these circumstances we need to perform long integrations and impose stringent convergence criteria as first done in Ref. [53].

We begin by writing $x(t) \equiv \tan[k\delta(t)/2]$. Equation (8) then becomes an inhomogeneous Riccati equation,

$$\dot{x} = a + 2\,\Omega\,x + b\,x^2, \tag{13}$$

where

$$a(t, \tilde{\alpha}, \gamma, \beta, k) \equiv -\frac{k}{\sqrt{2}}\tilde{\alpha} - 3\sqrt{2}k\gamma B(t) - \frac{3k}{2\sqrt{2}}\beta A\cos\phi,$$

$$b(t, \tilde{\alpha}, \gamma, \beta, k) \equiv -\frac{k}{\sqrt{2}}\tilde{\alpha} - 3\sqrt{2}k\gamma B(t) + \frac{3k}{2\sqrt{2}}\beta A\cos\phi,$$

$$\Omega(t, \beta, k) \equiv \frac{3k}{2\sqrt{2}}\beta A\sin\phi. \tag{14}$$

Next, using the Riccati transformation $x = -\dot{y}/[b(t)y]$, we find that the auxiliary variable $y(t)$ satisfies a damped second-order linear ordinary differential equation,

$$\ddot{y} - \left(2\,\Omega + \frac{\dot{b}}{b}\right)\dot{y} + a\,b\,y = 0, \tag{15}$$

which can in turn be transformed into an undamped Hill equation using the change of variable $y(t) = z(t)\exp[\xi(t)]$, where $\xi \equiv \int (2\Omega + \dot{b}/b)dt/2$:

$$\ddot{z} + \left\{\frac{\ddot{b}}{2b} - \frac{\dot{b}^2}{2b^2} - \frac{1}{4}\left(2\Omega + \frac{\dot{b}}{b}\right)^2 + ab\right\}z = 0. \tag{16}$$

This linear equation represents a parametrically driven oscillator with a frequency that fluctuates chaotically. Note that this frequency diverges at $b = 0$. Figure 6 shows that while b can indeed pass through zero, it does so infrequently. Moreover, since the term in braces, hereafter referred to as ω^2, is then large and negative the solution $z = 0$ is then strongly unstable and hence far from the pinning-depinning transition which remains unaffected.

In the following we study the boundedness of solutions of Eq. (16) as a function of the parameters, employing the strict convergence criteria developed for the stability of the $z = 0$ solution for quasiperiodic frequencies [53]. Specifically, we evolve the equation up to a maximum of 10^7 time steps. To define the notion of convergence, we introduce the radius $R(t) \equiv \sqrt{z(t)^2 + \dot{z}(t)^2}$ representing the instantaneous amplitude of the solution in phase space. A solution $z(t)$ will be called unbounded (bounded) if it exceeds (fails to exceed) $R_{\min} = 10^{-1}$ during an integration time of $0 \leqslant t \leqslant 10^7$. Unbounded
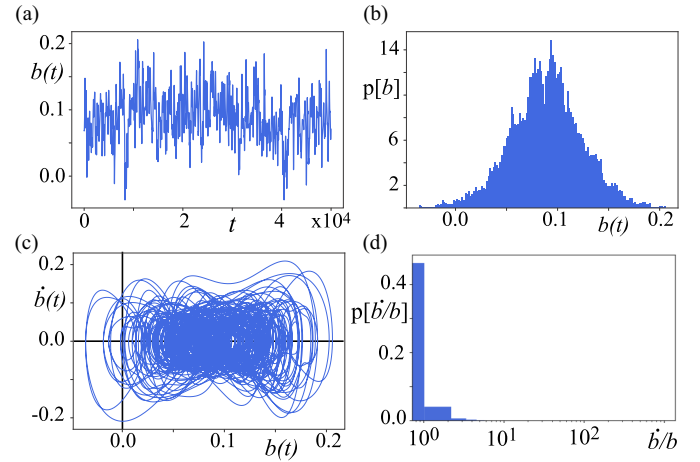

FIG. 6. Statistical characterization of the auxiliary function $b(t)$ defined in Eq. (14b). (a) Temporal evolution and (b) histogram of $b(t)$. (c) Reconstruction of the dynamics in $(b, \dot{b})$ space. (d) Probability density function of $\dot{b}/b$ in terms of a histogram.

trajectories $z(t)$ correspond to pinning in the original problem. In Fig. 7 the shaded (unshaded) region obtained in this manner corresponds to pinned (depinned) fronts.

A. Hill equation with chaotic frequency

To gain insight into the dynamics of the front position in the presence of chaotic forcing, we consider an overdamped pendulum, described by an angle θ and subject to the effect of a chaotic torque,

$$\dot{\theta} = -\sin\theta + r(t), \tag{17}$$

where $r(t) = r_0 + \xi X(t)$, r_0 and ξ are control parameters, and $X(t)$ is a zero-mean component of the Lorenz model [54], satisfying

$$\dot{X} = \sigma(Y - X), \quad \dot{Y} = X(\rho - Z) - Y, \quad \dot{Z} = XY - \beta Z. \tag{18}$$
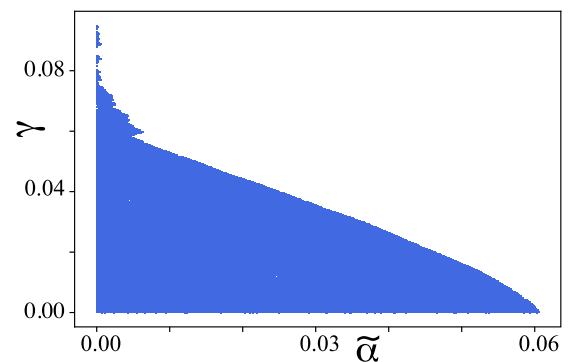

FIG. 7. Region with unbounded solutions (blue, pinned fronts) of the the Hill equation (16) shown in the $(\tilde{\alpha}, \gamma)$ parameter space, where $\tilde{\alpha} = \alpha_M - \alpha$. The equation has a chaotic frequency arising from B(t). Outside this region the solutions are bounded (depinned fronts). Parameters are $\beta = 0.085$ and $k = 0.7$.
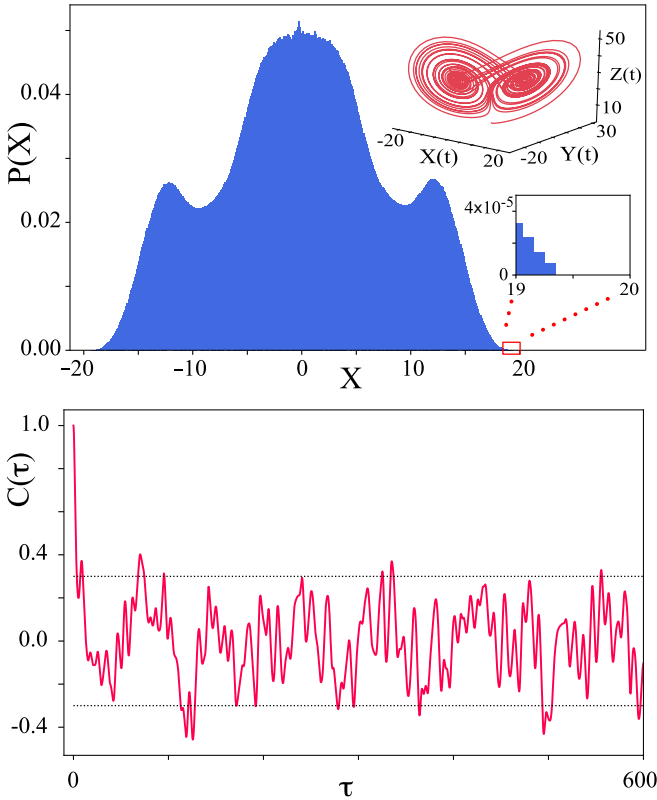
FIG. 8. Statistical characterization of the chaotic forcing function $X(t)$ showing the probability density distribution of $X(t)$ in the Lorenz model with $\beta = 8/3$, $\sigma = 10$, and $\rho = 28$. The top inset shows the corresponding strange attractor. The bottom inset shows a zoom of the tail of the probability distribution. (b) Correlation function $C(\tau) \equiv \langle X(t)X(t+\tau) \rangle$.

We employ the traditional parameter values $\beta = 8/3$, $\sigma = 10$, and $\rho = 28$ used by Lorenz to study the chaotic behavior of this system [54]. Note that $X(t)$ has a symmetric distribution about $X = 0$ and that its correlation function does not decay as shown in Fig. 8. These properties mimic the behavior of the effective forcing B(t) in Eq. (12), cf. Fig. 5. Moreover, the forced overdamped pendulum, Eq. (17), resembles Eq. (8) for the front position $\delta(t)$ in the sense that for $\xi = 0$ and $r_0 \leqslant 1$ ($r_0 > 1$) the trajectories of the pendulum in phase space are bounded (unbounded). However, when $\xi \neq 0$ and chaotic forcing is present the characterization of the stability of a trajectory in phase space becomes a nontrivial problem.

Using variable changes similar to those used to transform Eq. (8) into Eq. (16), that is, using $h \equiv \tan(\theta/2)$, $h = -2\dot{y}/[r(t)y]$, $y(t) = z(t)\exp[\xi(t)]$, where $\xi(t)$ is now given by $\xi = -\int (1 - \dot{r}/r)dt/2$, we can cast Eq. (17) into a Hill equation as well:

$$\ddot{z} + \left\{ \frac{\ddot{r}}{2r} - \frac{\dot{r}^2}{2r^2} - \frac{1}{4}\left(1 - \frac{\dot{r}}{r}\right)^2 + \left(\frac{r}{2}\right)^2 \right\}z = 0. \quad (19)$$

When the term in braces, i.e., the square of the instantaneous frequency ω^2, is a periodic function of time, it is well known that this equation has both bounded and unbounded solutions depending on the oscillation frequency [55,56]. This situation persists when the oscillation frequency is quasiperiodic but the boundary between bounded and unbounded solutions becomes a complex function of the parameters whose complete characterization remains an open problem [53]. In the present case $r(t)$ also occasionally passes through zero, but as in Eq. (16), this does not affect the pinning-depinning transition.

To study the boundedness of solutions of Eq. (19) as a function of the parameters, we employ the same strategy as in the previous section. Figure 9 depicts a sample trajectory
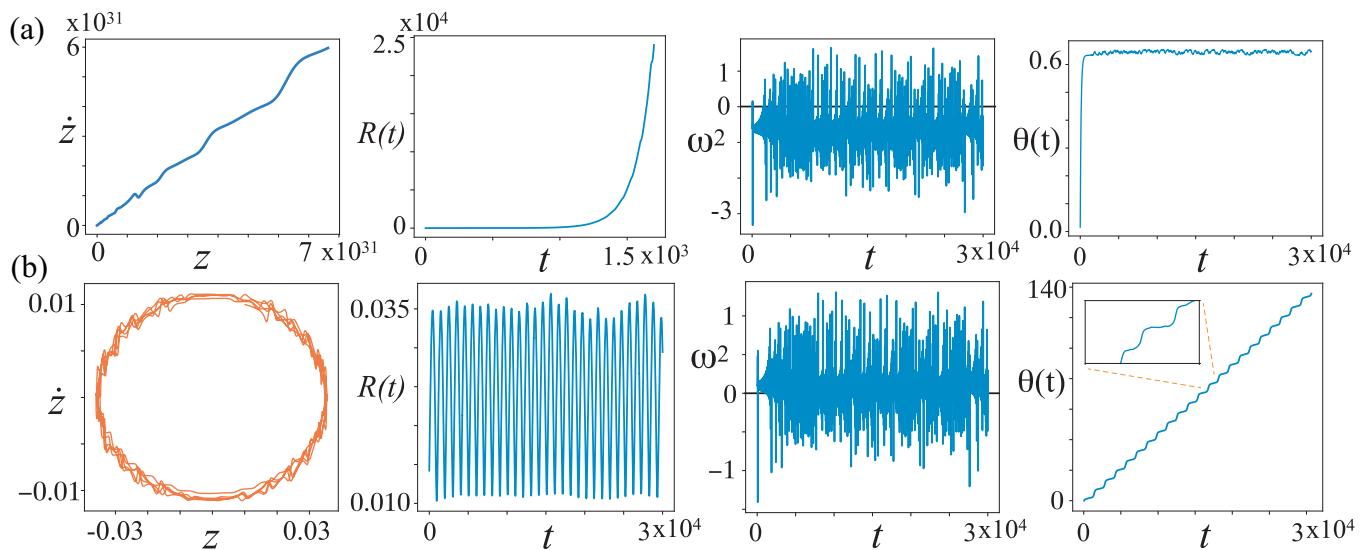

FIG. 9. Temporal evolution of the Hill equation (19) with Lorenz forcing computed for (a) $\xi = 0.001$, $r_0 = 0.6$ [$z(t)$ unbounded, $\theta(t)$ pinned] and (b) $\xi = 0.001$, $r_0 = 1.1$ [$z(t)$ bounded, $\theta(t)$ depinned]. The panels from left to right show the trajectory in the $(z, \dot{z})$ phase space, the temporal evolution of $R(t)$, the effective squared frequency ω^2 in the Hill equation, and the angle $\theta(t)$ reconstructed from the temporal evolution of $z(t)$ in the region of (a) pinning and (b) depinning.
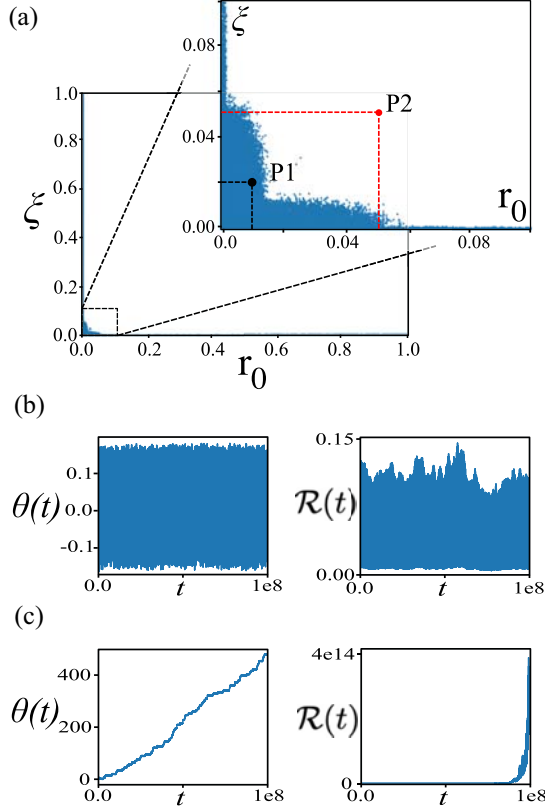
FIG. 10. (a) Parameter space of the Hill equation (19) with Lorenz forcing. Shaded (unshaded) regions correspond to pinned (depinned) fronts as determined by the condition $R(t) > 10^{-6}$ $[R(t) < 10^{-6}]$ in time $0 \leqslant t \leqslant 10^7$ analogous to that used in Eq. (16), starting from an initial condition with $R(0) = 10^{-9}$. (b), (c) Temporal evolution of $\theta(t)$ and the analogous quantity $\mathcal{R}(t) \equiv \sqrt{\theta(t)^2 + \dot{\theta}(t)^2}$ as obtained from Eq. (17) in the region of (b) pinning and (c) depinning, corresponding, respectively, to locations P_1 and P_2 in parameter space (a).

in the $(z, \dot{z})$ phase space, the temporal evolution of the radius $R(t) \equiv \sqrt{z(t)^2 + \dot{z}(t)^2}$, the coefficient $\omega^2(t)$ in the Hill equation (19), and the reconstructed variable $\theta(t)$ corresponding to (a) pinning, and (b) depinning. Observe that in (a) ω^2 is on average negative while in (b) it is positive.

Using this type of analysis, one can explore the parameter space of the problem and map out in detail the boundary between pinning and depinning within Eq. (17). Figure 10 summarizes this analysis in the (r_0, ξ) plane: blue points represent trajectories that diverge. The boundary between the trajectories that have and have not diverged is evidently complex, and remains to be characterized in detail. The figure also shows the evolution of $\theta(t)$ and the quantity $\mathcal{R}(t) \equiv \sqrt{\theta(t)^2 + \dot{\theta}(t)^2}$ obtained numerically from Eq. (17) in the region of (b) pinning and (c) depinning, respectively.

V. MULTIPLICATIVE NOISE INDUCES FRONT PROPAGATION

The first description of macroscopic matter is usually done using a small number of coarse-grained or macroscopic fields,
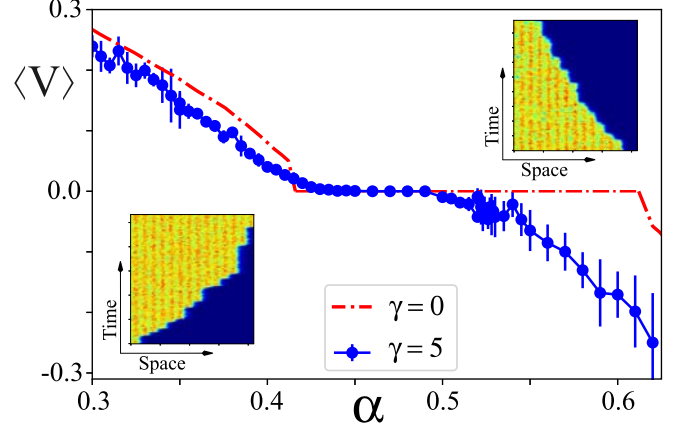

FIG. 11. Average speed of a front connecting homogeneous and pattern states as function of α for the stochastic model, Eq. (20), with $\beta = 0.085$ and $k = 0.7$. The red dot-dashed curve and the blue curve with filled circles show the deterministic and stochastic evolution of the front between a homogeneous and a periodic state, respectively. The insets show sample spatiotemporal evolution of the front before (lower left) and after (upper right) the Maxwell point when $\gamma = 5$.

whose evolution is described by deterministic differential equations. This reduction is a consequence of temporal scale separation, which allows a description in terms of the slowly varying macroscopic variables. An improved description includes fluctuations due to the elimination of a large number of fast variables whose effect can be modeled by including suitable inherent stochastic terms (or noise) in the differential equations. The stochastic term can be classified into two types: additive (multiplicative) noise that does not depend (depends) on the variable under study. Additive noise induces propagation of a static front connecting a stable homogeneous equilibrium and a pattern state [14,15]. The effect of multiplicative noise on fronts that connect a pair of homogeneous states has also been studied (see the textbook [57] and reference therein). In particular, the dynamic evolution of a system with fronts connecting an absorbing state (a state without fluctuations) and a fluctuating one has been discussed, and the emergence of spatiotemporal intermittency established [58].

In this section we compare the pinning-depinning results obtained with deterministic spatiotemporally chaotic forcing [Eqs. (1) and (2)] with the corresponding results obtained with explicitly stochastic forcing. In both cases the forcing is multiplicative. For this purpose we consider the following stochastic model:

$$\partial_t u = u(\alpha - u)(u - 1) + \partial_{xx} u + \beta u \cos(kx) + \gamma u \zeta(x, t),$$

(20)

where $\zeta(x, t)$ is a Gaussian white noise with zero mean value, $\langle \zeta(x, t) \rangle = 0$, and correlation $\langle \zeta(x, t)\zeta(x', t') \rangle = \delta(x - x')\delta(t - t')$. Here, the coefficient γ represents the noise strength, as in Eqs. (1) and (2), and the symbol $\langle \cdot \rangle$ indicates averaging over the realizations of the noise.

Since the noise in Eq. (20) is multiplicative and proportional to u, the state $u = 0$ is an absorbing state. In contrast,

the state $u = 1$ is an equilibrium state that exhibits persistent fluctuations. The front position $x = \delta(t)$ between these states exhibits random motion. Figure 11 shows the average front speed in the model. As a result of inherent fluctuations, one observes that the pinning region disappears and the front is only (statistically) stationary at a single point of the parameter space, the Maxwell point. The location of this point in turn depends on the intensity level γ of the noise. The disappearance of the pinning region in the present case is notable and is due to the fact that some realization of the stochastic process always overcomes the nucleation barrier introduced by the periodic forcing [15], a phenomenon known as a noise-induced transition [16].

To characterize this behavior one can use the same strategy as in Sec. III, and write down an equation for the front position $x = \delta(t)$. Using the ansatz (6) in Eq. (20), linearizing in W, and applying the appropriate solvability condition, one obtains

$$\dot{\delta} = -\frac{\partial U}{\partial \delta} + \Gamma \xi(t), \tag{21}$$

where the potential $U(\delta)$ is defined in expression (9), and

$$\xi(t) \equiv -\frac{3\gamma}{2\sqrt{\Gamma}} \int \zeta(z + \delta, t) u_F \, \partial_z u_F \, dz, \tag{22}$$

$$\Gamma \equiv \left(\frac{3\gamma}{2}\right)^2 \int [u_F(z)\partial_z u_F(z)]^2 \, dz = \frac{27\gamma^2}{40\sqrt{2}}. \tag{23}$$

Here, Γ measures the strength of the effective noise at the level of the front. Equation (21) is a Langevin equation for the front position with a Gaussian white noise. Specifically,

$$
\begin{aligned}
\langle \xi(t) \rangle &\equiv \left\langle -\frac{3\gamma}{2\sqrt{\Gamma}} \int \zeta(z + \delta, t) u_F \, \partial_z u_F \, dz \right\rangle, \\
&= -\frac{3\gamma}{2\sqrt{\Gamma}} \int \langle \zeta(z + \delta, t) \rangle u_F \, \partial_z u_F \, dz, \\
&= 0
\end{aligned}
\tag{24}
$$

with the same procedure for the other cumulants. In particular, $\langle \xi(t)\xi(t') \rangle = \delta(t - t')$. Thus all the properties of the reduced noise $\xi(t)$ are inherited from the spatiotemporal noise $\zeta(z, t)$. Note that in contrast to B(t) the noise $\xi(t)$ is not bounded, despite the presence of the cutoff represented by the term $\partial_z u_F(z)$ in the integrand in Eq. (22). This is because $\xi(t)$ depends on the noise realization, in addition to its time-dependence. This difference has profound consequences for the pinning-depinning transition.

Equation (21) describes an overdamped system with a ratchet potential and additive white noise. Owing to generic asymmetry of the potential U whenever $\alpha \neq 0$ and the lack of a global stationary state, the system continuously converts random fluctuations into directed motion of the front, i.e., the noise induces front propagation. This behavior is known as a Brownian motor [59]. Thus the main difference between chaotic and stochastic forcing is that the former exhibits a pinning-depinning transition while the latter does not.

VI. CONCLUSIONS AND REMARKS

The description of many-body systems using differential equations for macroscopic variables with fluctuating terms that account for ignored fast variables has been very successful. A classic example of this type of description is the Langevin equation associated with Brownian motion. This description assumes, explicitly or implicitly, that the fluctuations are incoherent and so can be modeled by a prescribed stochastic process. If the number of fast degrees of freedom is large this process is taken to be Gaussian white noise. In general one expects similar behavior in the presence of deterministic fluctuations arising from a chaotic or turbulent system. However, as shown here, there are important differences between these two descriptions when it comes to the dynamics of fronts. This is because the front profile provides a cutoff that determines the effective noise acting on the front. This cutoff, specified by the function $\partial_z u_F(z)$, acts like a smoothed out δ-function. Indeed, if we replace $\partial_z u_F(z)$ by $G\delta(z)$, we obtain from Eq. (12) the result B$(t) = Gu_F(0)\partial_z \psi(\delta, t)$ as the noise acting at the location $x = \delta$ of the front. Since $\psi(\delta, t)$ is specified by the bounded dynamics of the Kuramoto-Sivashinsky equation (2) B(t) represents bounded fluctuations which may or may not trigger a depinning transition. In contrast, in the stochastically driven system (20) a similar procedure leads to the expression $\xi(t) = G'u_F(0)\zeta(\delta, t)$. Since $\zeta(t)$ is a Gaussian white noise by assumption, we see that so is $\xi(t)$. However, the stochastic description allows rare but arbitrarily large fluctuations at any one location and this fact ultimately triggers a depinning transition—all that one has to do is wait long enough. This is not so in the deterministic case. We believe that it is this distinction between the effective noise at the front location that is ultimately responsible for the survival of pinning in the deterministic case and its disappearance in the stochastic case. This distinction may play a significant role in the evolution of macroscopic quantities in other circumstances as well, as in Ref. [60].

The dynamics of fronts is well known to be highly sensitive to details of the system just ahead of the front, as in the example studied by Brunet and Derrida [61,62] where departures from the continuum description were found to have an important effect on the speed of an invasion front. In this paper we have obtained a similar result and showed that deterministic spatiotemporal fluctuations can trigger a pinning-depinning transition of spatiotemporally chaotic patterns, a transition that is washed out when stochastic fluctuations are used instead. This fact represents a fundamental distinction between these two cases.

[1] L. M. Pismen, *Patterns and Interfaces in Dissipative Dynamics* (Springer Science & Business Media, Berlin, 2006).

[2] P. Collet and J. P. Eckmann, *Instabilities and Fronts in Extended Systems* (Princeton University Press, Princeton, NJ, 1990).

[3] M. C. Cross and P. C. Hohenberg, Pattern formation outside of equilibrium, Rev. Mod. Phys. **65**, 851 (1993).

[4] Y. Pomeau, Front motion, metastability and subcritical bifurcations in hydrodynamics, Phys. D (Amsterdam) **23**, 3 (1986).

[5] R. A. Fisher, The wave of advance of advantageous genes, Ann. Eugenics **7**, 355 (1937).

[6] A. N. Kolmogorov, I. G. Petrovsky, and N. S. Piskunov, A study of the diffusion equation with increase in the amount of substance, and its application to a biological problem, Bull. Moscow Univ. Math. Mech. **1**, 1 (1937).

[7] M. Faraday, *Course of Six Lectures on the Chemical History of a Candle* (Griffin, Bohn & Co, London, 1861).

[8] J. D. Murray, *Mathematical Biology* (Springer-Verlag, Berlin, 1989).

[9] J. S. Langer, Instabilities and pattern formation in crystal growth, Rev. Mod. Phys. **52**, 1 (1980).

[10] W. van Saarloos and P. C. Hohenberg, Fronts, pulses, sources and sinks in generalized complex Ginzburg-Landau equations, Phys. D (Amsterdam) **56**, 303 (1992).

[11] W. van Saarloos, Front propagation into unstable states, Phys. Rep. **386**, 29 (2003).

[12] J. Burke, and E. Knobloch, Localized states in the generalized Swift-Hohenberg equation, Phys. Rev. E **73**, 056211 (2006).

[13] F. Haudin, R. G. Elías, R. G. Rojas, U. Bortolozzo, M. G. Clerc, and S. Residori, Driven front Propagation in 1D Spatially Periodic Media, Phys. Rev. Lett. **103**, 128003 (2009).

[14] I. S. Aranson, B. A. Malomed, L. M. Pismen, and L. S. Tsimring, Crystallization kinetics and self-induced pinning in cellular patterns, Phys. Rev. E **62**, 5(R) (2000).

[15] M. G. Clerc, C. Falcon, and E. Tirapegui, Additive Noise Induces front Propagation, Phys. Rev. Lett. **94**, 148302 (2005).

[16] W. Horsthemke and R. Lefever, *Noise-Induced Transitions* (Springer-Verlag, Berlin/Heidelberg, 2006).

[17] T. Tsuruda and T. Hirano, Growth of flame front turbulence during flame propagation across an obstacle, Combus. Sci. Tech. **51**, 323 (1987).

[18] S. S. Shy, R. H. Jang, and P. D. Ronney, Laboratory simulation of flamelet and distributed models for premixed turbulent combustion using aqueous autocatalytic reactions, Combus. Sci. Tech. **113**, 329 (1996).

[19] S. Daniele, J. Mantzaras, P. Jansohn, A. Denisov, and K. Boulouchos, Flame front/turbulence interaction for syngas fuels in the thin reaction zones regime: turbulent and stretched laminar flame speeds at elevated pressures and temperatures, J. Fluid Mech. **724**, 36 (2013).

[20] D. Barkley, Theoretical perspective on the route to turbulence in a pipe, J. Fluid Mech. **803**, P1 (2016).

[21] A. Pocheau, Scale invariance in turbulent front propagation, Phys. Rev. E **49**, 1109 (1994).

[22] M. Anderson, F. Leo, S. Coen, M. Erkintalo, and S. G. Murdoch, Observations of spatiotemporal instabilities of temporal cavity solitons, Optica **3**, 1071 (2016).

[23] Z. Liu, M. Ouali, S. Coulibaly, M. G. Clerc, M. Taki, and M. Tlidi, Characterization of spatiotemporal chaos in a Kerr optical frequency comb and in all fiber cavities, Opt. Lett. **42**, 1063 (2017).

[24] Y. Kuramoto and D. Battogtokh, Coexistence of coherence and incoherence in nonlocally coupled phase oscillators, Nonlin. Phenom. Complex. Syst. (Dordrecht, Netherlands) **5**, 380 (2002).

[25] D. M. Abrams and S. H. Strogatz, Chimera States for Coupled Oscillators, Phys. Rev. Lett. **93**, 174102 (2004).

[26] C. R. Laing, Fronts and bumps in spatially extended Kuramoto networks, Phys. D (Amsterdam) **240**, 1960 (2011).

[27] M. G. Clerc, M. A. Ferré, S. Coulibaly, R. G. Rojas, and M. Tlidi, Chimera-like states in an array of coupled-waveguide resonators, Optics Lett. **42**, 2906 (2017).

[28] M. G. Clerc, S. Coulibaly, M. A. Ferré, and R. G. Rojas, Chimera states in a Duffing oscillators chain coupled to nearest neighbors, Chaos **28**, 083126 (2018).

[29] N. G. van Kampen, *Stochastic Processes in Physics and Chemistry* (Elsevier, New York, 1992).

[30] J. P. Eckmann and D. Ruelle, Ergodic theory of chaos and strange attractors, in *The Theory of Chaotic Attractors* (Springer-Verlag, New York, 1985), pp. 273–312.

[31] N. Verschueren, U. Bortolozzo, M. G. Clerc, and S. Residori, Chaoticon: Localized pattern with permanent dynamics, Phil. Trans. R. Soc. A **372**, 20140011 (2014).

[32] Y. Kuramoto and T. Tsuzuki, On the formation of dissipative structures in reaction-diffusion systems: Reductive perturbation approach, Prog. Theor. Phys. **54**, 687 (1975).

[33] Y. Kuramoto and T. Tsuzuki, Persistent propagation of concentration waves in dissipative media far from thermal equilibrium, Prog. Theor. Phys. **55**, 356 (1976).

[34] Y. Kuramoto, Diffusion-induced chaos in reaction systems, Prog. Theor. Phys. Supplement **64**, 346 (1978).

[35] D. M. Michelson and G. I. Sivashinsky, Nonlinear analysis of hydrodynamic instability in laminar flames-I. Derivation of basic equations, Acta Astronautica **4**, 1177 (1977).

[36] D. M. Michelson and G. I. Sivashinsky, Nonlinear analysis of hydrodynamic instability in laminar flames-II. Numerical experiments, Acta Astronautica **4**, 1207 (1977).

[37] Y. Kuramoto, *Chemical Oscillations, Waves, and Turbulence* (Springer Science & Business Media, New York, 2012).

[38] M. G. Clerc, D. Escaff, and V. M. Kenkre, Patterns and localized structures in population dynamics, Phys. Rev. E **72**, 056217 (2005).

[39] F. Haudin, R. G. Elías, R. G. Rojas, U. Bortolozzo, M. G. Clerc, and S. Residori, Front dynamics and pinning-depinning phenomenon in spatially periodic media, Phys. Rev. E **81**, 056203 (2010).

[40] B. C. Ponedel and E. Knobloch, Forced snaking: Localized structures in the real Ginzburg-Landau equation with spatially periodic parametric forcing, Eur. Phys. J. Special Topics **225**, 2549 (2016).

[41] U. Thiele and E. Knobloch, Driven Drops on Heterogeneous Substrates: Onset of Sliding Motion, Phys. Rev. Lett. **97**, 204501 (2006).

[42] M. G. Clerc, R. G. Elías, and R. G. Rojas, Continuous description of lattice discreteness effects in front propagation, Phil. Trans. R. Soc. A **369**, 412 (2011).

[43] A. Pikovsky and A. Politi, *Lyapunov Exponents: A Tool to Explore Complex Dynamics* (Cambridge University Press, Cambridge, 2016).

[44] G. Nicolis, *Introduction to Nonlinear Science* (Cambridge University Press, Cambridge, 1995).

[45] F. Christianen and H. H. Rugh, Computing Lyapunov spectra with continuous Gram-Schmidt orthonormalization, Nonlinearity **10**, 1063 (1997).

[46] T. J. Bridges and S. Reich, Computing Lyapunov exponents on a Stiefel manifold, Phys. D (Amsterdam) **156**, 219 (2001).

[47] E. I. Fredholm, Sur une classe d'equations fonctionnelles, Acta Math. **27**, 365 (1903).

[48] R. Peierls, The size of a dislocation, Proc. Phys. Soc. **52**, 34 (1940).

[49] F. R. N. Nabarro, Dislocations in a simple cubic lattice, Proc. Phys. Soc. **59**, 256 (1947).

[50] F. R. N. Nabarro, *Theory of Crystal Dislocations* (Dover Publications, Inc., New York, 1947).

[51] M. G. Clerc, S. Coulibaly, M. A. Ferré, M. A. García-Ñustes, and R. G. Rojas, Chimera-type states induced by local coupling, Phys. Rev. E **93**, 052204 (2016).

[52] P. Gandhi, E. Knobloch, and C. Beaume, Dynamics of phase slips in systems with time-periodic modulation, Phys. Rev. E **92**, 062914 (2015).

[53] R. S. Zounes and R. H. Rand, Transition curves for the quasi-periodic Mathieu equation, SIAM J. Appl. Math. **58**, 1094 (1998).

[54] E. N. Lorenz, Deterministic nonperiodic flow, J. Atmos. Sci. **20**, 130 (1963).

[55] A. H. Nayfeh and D. T. Mook, *Nonlinear Oscillations* (John Wiley & Sons, New York, 2008).

[56] W. Magnus and S. Winkler, *Hill's Equation* (Dover Publications Inc., New York, 2004).

[57] J. García-Ojalvo and J. Sancho, *Noise in Spatially Extended Systems* (Springer Science & Business Media, New York, 2012).

[58] M. G. Zimmermann, R. Toral, O. Piro, and M. San Miguel, Stochastic Spatiotemporal Intermittency and Noise-Induced Transition to an Absorbing Phase, Phys. Rev. Lett. **85**, 3612 (2000).

[59] P. Reimann, Brownian motors: Noisy transport far from equilibrium, Phys. Rep. **361**, 57 (2002).

[60] C. Chatelain, P. E. Berche, and B. Berche, Second-order phase transition induced by deterministic fluctuations in aperiodic eight-state Potts models, Eur. Phys. J. B **7**, 439 (1999).

[61] E. Brunet and B. Derrida, Shift in the velocity of a front due to a cutoff, Phys. Rev. E **56**, 2597 (1997).

[62] E. Brunet and B. Derrida, Effect of microscopic noise on front propagation, J. Stat. Phys. **103**, 269 (2001).